# Flow transients in un-started and started modes of vacuum ejector operation

R. Arun Kumar and G. Rajesh

Citation: Phys. Fluids **28**, 056105 (2016); doi: 10.1063/1.4948959
View online: http://dx.doi.org/10.1063/1.4948959
View Table of Contents: http://aip.scitation.org/toc/phf/28/5
Published by the American Institute of Physics

PHYSICS OF FLUIDS **28**, 056105 (2016)

# Flow transients in un-started and started modes of vacuum ejector operation

R. Arun Kumar and G. Rajesh[a)]
*Department of Aerospace Engineering, Indian Institute of Technology Madras, Chennai 600036, India*

(Received 8 January 2016; accepted 28 April 2016; published online 23 May 2016)

An experimental study has been carried out to investigate the nature of transients in vacuum ejector flows during start-up and the dynamics in flow characteristics. The results show that the secondary stream induction progresses with non-uniform rates with the ramping primary jet pressure during start-up. The initial evacuation period is subjected to gradual and highly perturbed secondary fluid entrainment. In this phase, the secondary stream induction by the shear layer is asymmetric leading to an un-even vacuum generation in the secondary chamber. In the second phase, the secondary pressure fluctuations are found to be ceased for a critical primary jet pressure followed by a rapid induction of the secondary fluid till the primary jet expands to the diffuser wall. The transition from the first phase to the second phase is caused by the secondary stream flow choking in the diffuser. Following the second phase, a stable stage exists in the third phase in which the vacuum pressure decreases only marginally. Any further attempt to increase the secondary chamber vacuum level beyond the third phase, by increasing the primary jet total pressure, results in flow reversal into the secondary chamber, spoiling the already achieved vacuum level. In the fourth phase of start-up, a complicated shock interaction transformation from a Mach reflection (MR) to regular reflection (RR) occurs within the diffuser. It is also observed that the primary jet pressures for the minimum secondary chamber pressure, the minimum secondary pressure, and the primary pressure for MR-RR transformation decrease initially with increase in diffuser length and then increase. It is found that the decreasing and increasing trends are caused by the pressure recovery and Fanno effects, respectively. *Published by AIP Publishing.* [http://dx.doi.org/10.1063/1.4948959]

## I. INTRODUCTION

Ejectors are devices that are primarily used for mixing two fluid streams or for transporting fluids by utilizing the energy of a fast moving primary jet. A conventional ejector system consists of a primary duct carrying high pressure fluid, a secondary duct, a straight diffuser (mixing chamber), and a subsonic diffuser.[1] Compared to the secondary duct inlet, the straight diffuser inlet experiences a low pressure due to the expansion of primary jet. This pressure difference along with the turbulent entrainment through the shear layer provides the driving force for the secondary stream induction. Ejector systems are widely used in situations where high pressure stream is already available and the associated flow energy can be utilized to mix and transport fluids by designing suitable aerodynamic passages. One such application is in combustion facilities, where ejectors are commonly used to mix fuel and oxidizers through the shearing action of two streams.[2] In refrigeration systems, the ejector principle is being used to drag the evaporator fluid using a primary jet with high momentum.[3–5] Ejectors are also used in thrust augmentation[6,7] and noise reduction[8] applications.

a)Electronic mail: rajesh@ae.iitm.ac.in

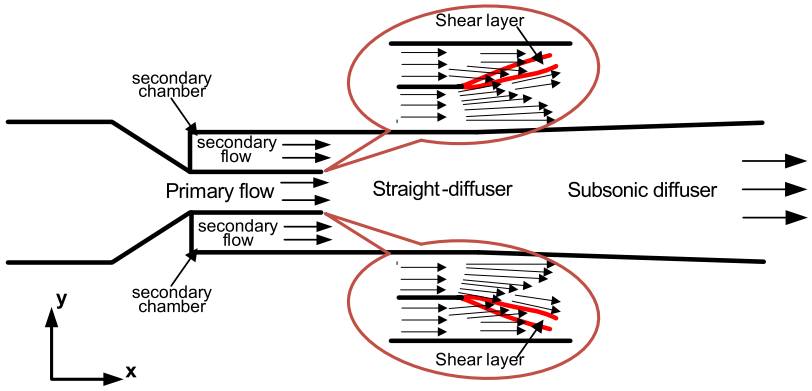


FIG. 1. Schematic of vacuum ejector-diffuser system.

Flow characteristics of conventional ejectors with constant secondary fluid supply are relatively well understood and documented in many past studies.[9–13] One of the most important applications of the ejector as a mass transport device is in vacuum generation, and such ejectors are called as vacuum ejectors or zero secondary flow ejectors. Schematic of a typical vacuum ejector-diffuser system is shown in Figure 1. In conventional ejectors, a constant supply of secondary stream is always maintained either by an external source or by a natural induction process, where as in vacuum ejectors, this is not possible due to the presence of a closed secondary chamber. As a result of this, the secondary chamber pressure reduces and reaches a steady state as the primary jet momentum increases due to the induction of secondary mass contained within the closed secondary chamber. Vacuum ejectors are primarily used to create controlled vacuum exit conditions in high altitude testing (HAT) of rocket engines.[14] Vacuum ejectors are also used in hypersonic test facilities to generate large pressure ratios (by reducing the exit pressures to very low levels) required for hypersonic Mach numbers are generated by reducing the exit pressure conditions to low vacuum levels.[15] The present work is aimed at understanding various operational modes of the vacuum ejector-diffuser systems.

The flow evolution and attainment of steady state are relatively more complex in vacuum ejectors as the secondary stream entrainment is strongly coupled with the primary jet expansion characteristics and vice versa.[16] Many of the earlier researches on vacuum ejectors focused primarily on the steady state flow characteristics such as the level of vacuum attainable in the secondary chamber and the parameters to optimize this.[17–21] In previous studies,[17,18] the vacuum ejector operations are classified as un-started and started depending on the amount of primary jet expansion. An ejector is said to be operating in un-started mode when the expanded primary jet does not reach to the straight-diffuser wall. Ejector operates in started mode when the expanded primary jet reaches to the straight-diffuser wall. In un-started mode, the secondary stream passage is open to straight-diffuser section, where the pressure recovery starts, whereas in the started mode, it is closed by the primary jet impinging the straight-diffuser wall as shown in Figures 2(a) and 2(b), respectively. Started mode operation is normally achieved by operating the vacuum ejector with primary jet total pressure ($P_0$) above a critical value, termed as starting mode pressure, which can be determined analytically using isentropic and normal shock relations.[21,22] This analytical treatment assumes that the pressure recovery in the diffuser duct through a series of oblique shock waves is nearly equivalent to the pressure rise produced by a single normal shock wave with the same primary jet Mach number at diffuser inlet.[23] The inlet to the diffuser at started mode is taken as the section where the primary jet impinges the diffuser wall and is schematically shown in Figure 2(b). An experimental study by German and Bauer[21] reported that starting mode pressure ratio (primary jet total pressure ($P_0$)/static pressure at diffuser exit ($P_2$)) predicted using the normal shock assumption is valid only if the diffuser length to diffuser diameter ratio (L/D) is above an optimum value $(L/D)_{opt}$. If $L/D < (L/D)_{opt}$, the actual starting pressure condition required is much higher than the theoretically predicted value. They also reported that $P_0/P_2$ decreases with an increase in diffuser length, up to certain critical length and it remains constant thereafter, with increase in diffuser length.

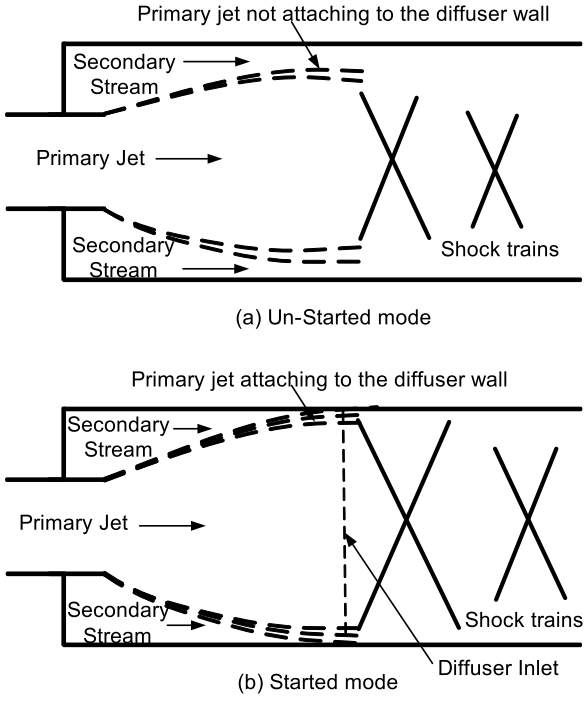


FIG. 2. Schematic of started and un-started modes of vacuum ejector operation.

There are many such parametric studies as above in the past to optimize the vacuum ejector performance. An experimental study carried out by Annamalai *et al.*[22] investigated the effect of parameters such as the ratio of the diffuser area to primary nozzle throat, diffuser area to primary nozzle exit area, diffuser length to its diameter, and the specific heat ratio of the driving gases on the minimum starting mode pressure ratio. Their results show that the starting pressure ratio increases when the diffuser to nozzle throat area ratio and the specific heat ratio of driving gas increase. In addition, they observed large pressure oscillations in the vacuum chamber during the un-started mode of ejector operation; but the reasons for this were not clearly reported. A recent study by Ashok *et al.*[24] proposed some measures such as provisions for back flow arresters and increasing the thickness of the nozzle lip to reduce the fluctuations in vacuum pressure. A numerical study by Kumaran *et al.*[25] showed that the usage of a second throat diffuser system improves the performance of vacuum ejectors. They also reported that the secondary chamber pressure level decreases with increase in primary jet mass flow rate up to a critical value and then increases with increase in primary jet mass flow rate.

All of the above studies were focused mainly on the performance of vacuum ejectors and tried to enhance vacuum levels through parametric variation in ejector configuration and flow properties without paying attention to the evolution of the transient flow fields. Attempts towards understanding the evolution of transient flow fields can be seen in more recent works.[16,26,27] In both un-started and started modes of operation of the vacuum ejector, the flow has to reach a steady state[28] where there is no more mass induction from the secondary chamber. This is referred to as dynamic pressure equilibrium, at the onset of which, recirculation zones develop in the secondary stream.[26] Though there is no more secondary fluid induction when the vacuum ejector flow reaches a steady state, the shear layer still persists through the recirculation process. Damped oscillations are reported in a numerical study conducted by Mittal *et al.*[16] in the secondary chamber pressure during the induction process, owing to the formation of a highly dynamic separation bubble in the secondary stream. Repeated flow reversals into the secondary chamber are also observed and corresponding flow oscillations are attributed to the extension and retraction of the separation bubble caused by transient characteristic changes in the primary jet shock structure.

It is now known that the vacuum levels in the secondary chamber reach a ceiling, specific to the configuration and flow parameters of the ejectors from the past studies, and the reasons for which are not sufficiently explained. This behavior of the vacuum ejectors is attributed to the dynamic characteristics of the flow evolution during start-up in some of the works based on scattered numerical data. In addition to the secondary vacuum level ceiling, there are other transient flow characteristics which are of relevance in vacuum ejector flows, especially for vacuum ejectors used in high altitude testing facilities. Generally for a HAT facility, the rocket nozzle plume acts as the primary jet and its expansion into a confined duct with upstream side closed produces the required low back pressure conditions. For HAT facilities, the primary jet expansion will be restricted by the geometry of the diffuser duct, whereas in actual flight scenario, the rocket nozzle plume (primary jet) is open to ambient conditions and is free to expand. Hence the plume characteristics and the performance of rocket nozzles predicted using HAT facilities may have discrepancies with the actual flight data. It hence becomes important to investigate the transient flow characteristics in the vacuum ejector diffuser section to envisage such discrepancies. A numerical study by Park *et al.*[29] provides some insights into the evolution of flow in the diffuser section during the starting and closing of vacuum ejectors. They observed that the starting and closing shock structures in the diffuser section are not the same and there exists a hysteresis in shock wave characteristics for the same pressure ratio conditions.

From the above literatures, the important aspects of the ejector flows can be broadly classified into (i) the vacuum level ceiling, (ii) the dynamic characteristics of the primary and secondary jets, and (iii) the coupling between the former and the latter. While there are a lot of research works in the form of parametric studies to estimate the vacuum ceiling levels at started condition and thereby enhancing the system performance, research works on other two aspects are relatively sparse. Moreover, the investigation on the dynamic primary-secondary flow interaction during the un-started mode will be important for vacuum ejector applications involved in refrigeration system, since for these applications, it is desired to operate the vacuum ejector at un-started mode. To the authors' best knowledge, most of the past studies investigating the vacuum ejector flow evolution characteristics[16,26,27] relied upon numerical data to resolve the transient flow fields while a few experimental studies[22,27] used pressure data in ejector system to quantify the transient effects. The coupling between the vacuum levels in the secondary chamber and the transient flow structures has never been investigated comprehensively elsewhere. Hence the primary motive of the current study is to investigate the transient characteristics of the diffuser flow evolution during the primary jet ramping process. The study also aims at understanding how the flow evolution decides the vacuum ceiling and the primary and secondary jet structures in the started and un-started ejector modes of operation and in the transformation phase, using experimental techniques. Unsteady pressures have been captured in the secondary chamber and along the diffuser wall, and the transient flow field is visualized using time resolved schlieren imaging technique. The flow visualization images are correlated to the pressure histories in the secondary as well as primary jet to investigate coupling between the vacuum levels and the transient flow structures in the flow field.

## II. EXPERIMENTAL SETUP

The experimental setup consists of a two dimensional vacuum ejector model with a straight primary duct, a closed secondary chamber (vacuum chamber), and a straight diffuser/mixing section, as shown in Figure 3(a). Ratio of the diffuser height (D) to the primary duct exit height (d) for the current geometry is 2.82. The primary duct is supplied with high pressure air using the open jet facility available at Department of Aerospace Engineering, IIT Madras as schematically shown in Fig. 3(b). Vacuum ejector is started by suddenly opening the primary jet valve in the open jet facility to the required settling chamber pressure and allowing the primary jet to expand into the diffuser section. During start-up, when the primary jet is choked at the primary duct exit, an under expanded jet is produced in the diffuser section. Various experiments have been carried out by starting the vacuum ejector with different primary jet total pressures and with different diffuser lengths. Test matrix for experimental cases is shown in Table I. Since large numbers of experiments were conducted to get numerous data points, only the major experimental cases which have been used for explaining the flow physics are shown in Table I.

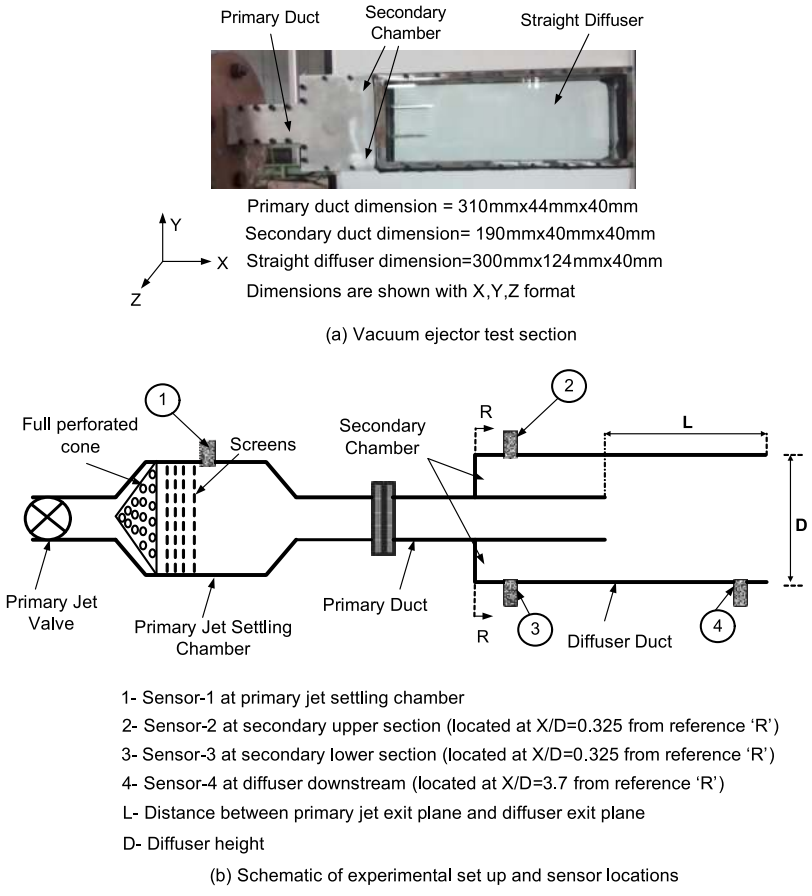


FIG. 3. Vacuum ejector-diffuser experimental setup.

The flow transients in the diffuser section during the primary jet total pressure ramping process were visualized using a time resolved schlieren technique. A conventional Z-type schlieren system with a vertical knife-edge was used to capture the density gradients in the stream wise direction (X-direction in Figure 3(a)). High speed imaging was done using PHOTRON FASTCAM SA-4 camera with 3600 frames/s at 10 $\mu$s exposure. Pressure variations in the secondary chamber and in the diffuser were measured using KELLER 21 P1Y (0-10 bars (absolute)) series piezo-resistive transmitter and the primary jet settling chamber pressure was measured using KELLER PAA 21Y (0-20 bars (absolute)) series piezo-resistive transmitter. The pressure data were acquired with a sampling frequency of 2 kHz. The sensitivity of the transducer is 0.9 V/bar. Uncertainty is ±0.5% of Full scale output (FSO). Locations of the pressure sensors are shown in Figure 3(b).

TABLE I. Operating conditions for various experimental cases with L/D = 2.5.

| Cases | Ratio of primary jet total pressure ($P_0$) to ambient pressure ($P_a$) |
|---|---|
| 1 | 2.1 |
| 2 | 2.6 |
| 3 | 3.3 |
| 4 | 4.2 |
| 5 | 4.8 |
| 6 | 5.2 |
| 7 | 6.4 |
| 8 | 6.75 |

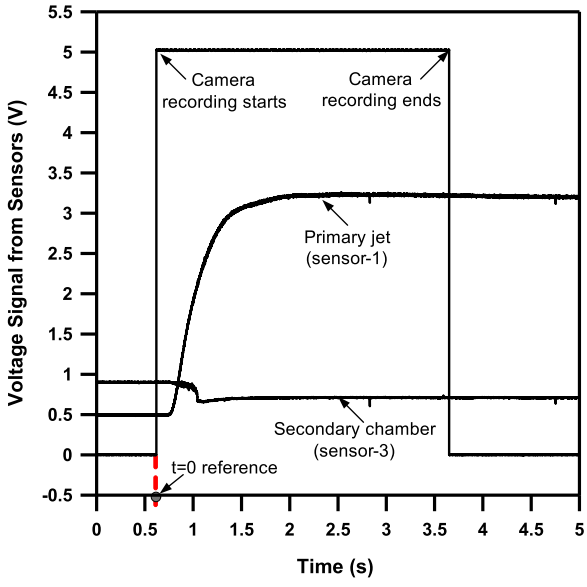


FIG. 4. Voltage signals from the sensors and camera with reference condition.

In the present experimental study, the flow evolution characteristics during vacuum ejector start-up have been investigated by correlating the secondary chamber pressure and primary jet total pressure with the time resolved schlieren images. In order to achieve this, a reference time has been defined and the following sequence has been followed. The pressure acquisition has been started at first followed by the camera recording and the primary jet pressure ramping by opening the valve in the blow down facility. Time elapsed between the beginning of the pressure acquisition and the camera triggering has been determined by fetching a digital output signal from the camera, as it is triggered. The time at which the camera output shows a steep increase has been identified as the reference time (t = 0) for all the data acquisitions. The process is shown in Figure 4, where the voltage signals from sensors and camera are plotted with respect to flow time.

## III. RESULTS AND DISCUSSION

Figure 5 shows the static pressure variation in the secondary chamber with respect to the primary jet pressure ramping for case-7 ($P_0$ = 6.4 bars). It can be observed from Figure 5 that the secondary

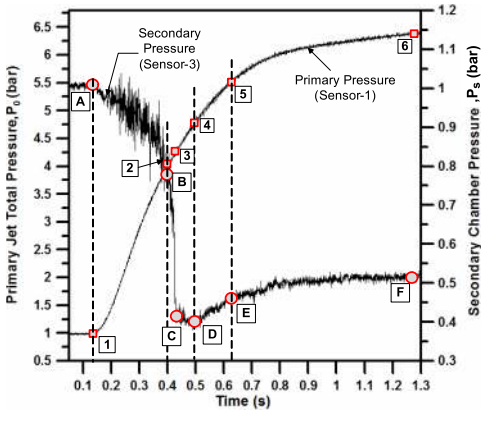


FIG. 5. Secondary chamber pressure-time history during primary jet ramping process (case-7).

chamber vacuum pressure varies in a non-monotonic fashion in time with four distinct phases of pressure changes. The initial phase, "A-B" (phase-1) in Figure 5, shows large scale pressure fluctuations in the secondary chamber. This shows that the secondary jet entrainment progresses in a perturbed manner in this phase, indicating the possibility of re-circulating flow to and from the secondary chamber. As the primary jet ramping pressure progresses to a critical value, point-2 in Figure 5, the secondary chamber pressure perturbations vanish (point-B in Figure 5). A rapid evacuation of the secondary chamber takes place thereafter. This rapid evacuation phase, "B-C" (phase-2) in Figure 5, continues till the primary jet expands to the diffuser wall and this marks the switching of un-started vacuum ejector operation to started vacuum ejector operation, as pointed out by previous researchers.[17,18] The starting mode pressure is shown as point-3 in Figure 5. After this, there is a small primary jet pressure window over which the secondary pressure reduces only marginally, and this phase is marked as "C-D" (phase-3) in Figure 5. Increasing the primary jet pressure from this state deteriorates the already existing secondary chamber vacuum pressure and this phase is marked as "D-F" (phase-4) in Figure 5. A detailed discussion on the flow characteristics during all the above phases of vacuum ejector operations is provided in Secs. III A–III D.

### A. Phase-1 vacuum ejector operation (L/D = 2.5)

For detailed investigation of phase-1 of the vacuum ejector operation, the primary jet total pressure has been varied in such a way that only phase-1 flow characteristics exist in the vacuum ejector (cases with $P_0$ = 2.1, 2.6, and 3.3 bars). The critical primary jet pressure up to which secondary chamber pressure exhibits oscillations can be obtained from point-2 in Figure 5. From the schlieren pictures (Figures 6(b), 8(b), and 11(b)), it can be observed that with a primary jet total pressure below that of point-2, the vacuum ejector always operates in the un-started mode. Case-1 ($P_0$ = 2.1 bars) represents such a situation and the corresponding static pressure-time histories in the secondary chamber and diffuser section are shown in Figure 6(a). It can be observed from Figure 6(a) that as primary jet pressure increases the secondary chamber vacuum level (sensor-3) also increases. This is as expected since an increase in primary jet total pressure increases the primary jet momentum and this, in turn, increases the secondary fluid induction. Figure 6(a) clearly depicts the secondary chamber pressure oscillations (sensor-3) during the first phase of evacuation process. Previous experimental study by Annamalai *et al.*[22] also reported such pressure oscillations for vacuum ejectors operated in the un-started mode. However, they did not provide any reason for these pressure oscillations.

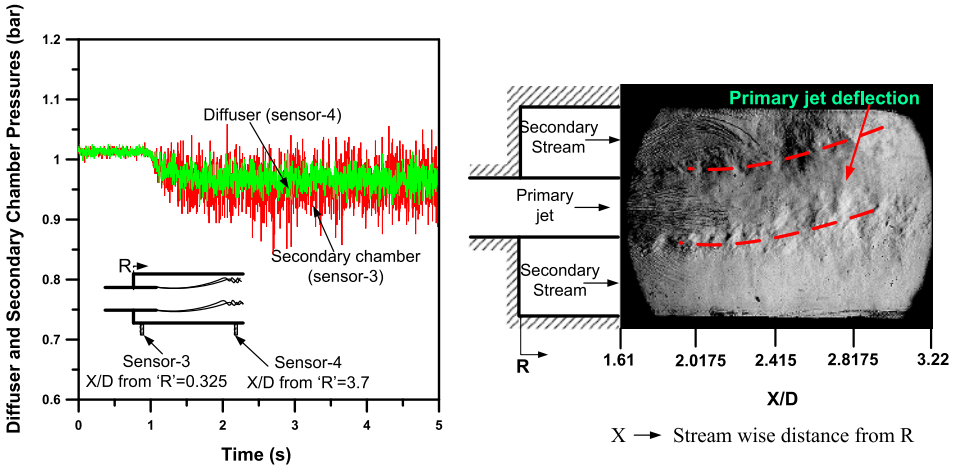


(a) Pressure histories in the secondary chamber and diffuser during vacuum ejector start-up (case-1)

(b) Schlieren image showing the preferential jet attachment of primary jet to the diffuser upper wall (case-1)

FIG. 6. Secondary and diffuser pressure histories and diffuser schlieren flow field (case-1).

These large scale pressure fluctuations can be noticed in the diffuser downstream side too (sensor-4) as seen in Figure 6(a). The schlieren picture for case-1 ($P_0 = 2.1$ bars), shown in Figure 6(b), reveals that the primary jet as well as the shear layer deflects upward in the diffuser section. Repeated experiments with different primary jet total pressure values show that the diffuser wall to which the primary jet deflects is a choice of the flow (Figures 6(b), 8(b), and 11(b)). In the past, researches on low Reynolds number symmetric duct flows with sudden expansion also reported such asymmetric expansions.[30–32] They attributed this phenomenon to the existence of asymmetric recirculation bubbles in the upper and lower sides of the expanding jet. The primary jet deflection seen in the present experimental study suggests the possibility of such recirculation bubbles in the secondary stream. The recirculation bubbles cause pressure perturbations in the diffuser downstream section. These perturbations may induce pressure oscillations in the secondary chamber in the un-started mode of ejector operation in which secondary chamber is open to the diffuser section.

In order to further investigate the influence of diffuser recirculation bubbles (sensor-4) on secondary pressure perturbations (sensor-3), the pressure fluctuation data from sensor-4 and sensor-3 have been correlated using Eq. (1). The cross correlation coefficients for the two pressure-time series for various time lags (delays) between sensor-3 data and sensor-4 data have been estimated and are presented in Figure 7. Figure 7(a) reveals that for case-1, the pressure fluctuations in sensor-3 are moderately correlated to the pressure fluctuations in sensor-4 very close to zero lag condition and not correlated at higher lag values. Since the two pressure-time series are not well correlated with each other, the secondary pressure perturbations during un-started mode are not solely determined by the diffuser re-circulation bubbles, but there could be more factors which affect the secondary pressure perturbations.

For various delays "d," cross correlation

$$r = \frac{\sum_i [(x_i - mx) * (y_{i-d} - my)]}{\sqrt{\sum_i (x_i - mx)^2} \sqrt{\sum_i (y_{i-d} - my)^2}}, \tag{1}$$

where $i = 0, 1, 2, \ldots, N-1$; $\pm d = 0, 1, 2, \ldots, N-1$,

$x_i$ = time series of secondary chamber pressure (sensor-3),
$mx$ = mean of secondary pressure time series (sensor-3),
$y_i$ = time series of diffuser chamber pressure (sensor-4),
$my$ = mean of diffuser pressure time series (sensor-4).

An experimental study with a primary jet total pressure of 3.3 bars (case-3) shows that the primary jet deflects downward in the diffuser section (to the side to which diffuser sensor

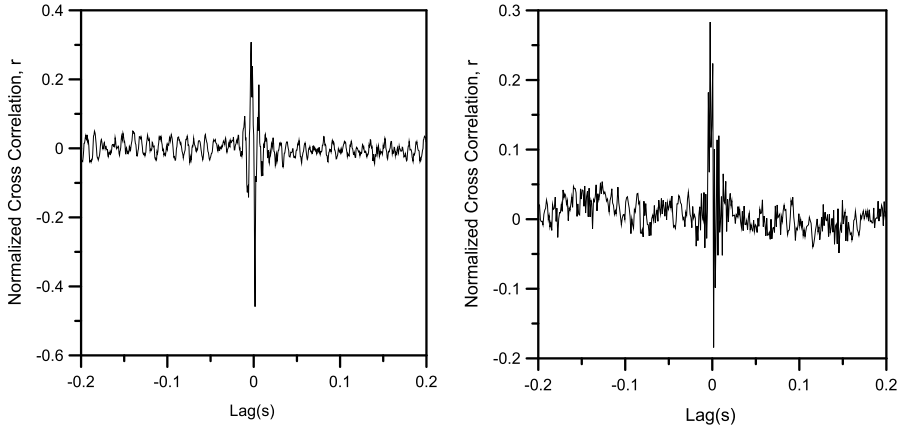


(a) Cross correlation between secondary and diffuser pressure fluctuations for case-1

(b) Cross correlation between secondary and diffuser pressure fluctuations for case-3

FIG. 7. Cross correlation between secondary and diffuser pressure fluctuations at various lags (cases-1 and 3).

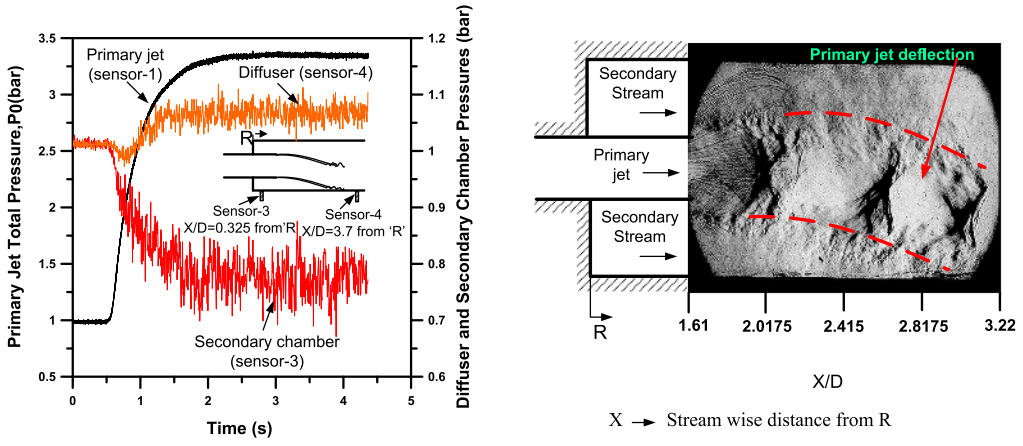


(a) Pressure histories in the secondary chamber and diffuser during vacuum ejector start-up (case-3)

(b) Schlieren image showing the preferential jet attachment of primary jet to the diffuser lower wall (case-3)

FIG. 8. Secondary and diffuser pressure histories and diffuser schlieren flow field (case-3).

(sensor-4) is located), unlike the case with $P_0$ = 2.1 bars, where the primary jet deflects upward. This can be observed from the diffuser schlieren image shown in Figure 8(b). As a result of the primary jet attachment with the diffuser bottom wall, the recirculation bubbles in the diffuser lower section will be confined to the upstream of the primary jet attachment point. After the attachment point, primary jet flow prevails along the diffuser bottom wall. Due to sufficiently large momentum of the primary jet flow, the possibility of a re-circulation bubble in the diffuser lower section downstream of the attachment point is sparse. It is seen that the primary jet attaches to the diffuser bottom wall at X/D ~ 3 (Figure 8(b)), whereas the diffuser sensor is located at X/D = 3.7 (Figure 8(a)). Hence the pressure perturbations observed in the diffuser sensor (sensor-4), shown in Figure 8(a), might not be induced by the re-circulation bubbles but due to the flow turbulence produced by the primary jet interaction with the diffuser wall. The pressure data for the case ($P_0$ = 3.3 bars), shown in Figure 8(a), reveal that the secondary chamber pressure (sensor-3) also shows large amplitude oscillations comparable to that of case-1 ($P_0$ = 2.1 bars). Cross correlation between the secondary pressure time data (sensor-3) and the diffuser pressure time data (sensor-4) for case-3, shown in Figure 7(b), shows a moderate correlation very close to zero lag. This suggests that the secondary chamber perturbations can also be influenced by the flow turbulence produced by the primary jet-wall interactions along with the re-circulation zones in the secondary stream. Cross correlation results from the two experimental cases (case-1 and case-3) thus suggest that the secondary chamber will be exposed to all kind of perturbations from the diffuser downstream section in the un-started mode, resulting in secondary pressure oscillations.

A computational fluid dynamics (CFD) simulation has also been carried out to confirm the presence of re-circulation bubbles in the diffuser section. The computational domain was discretized using quadrilateral cells. Grid independence study shows that a grid independent solution exists with a grid size of 143 847 cells and this grid is used for all CFD studies. The steady flow fields have been resolved by solving two-dimensional, compressible, Reynolds veraged Navier-Stokes equations using a commercial CFD solver, ANSYS FLUENT 14.0. Turbulence was modeled using SST k-ω model. Pressure inlet boundary condition has been used at the primary jet inlet with various primary jet total pressures. An extended computational domain has been created at the diffuser exit in order to specify the atmospheric pressure outlet boundary condition. A schematic of computational domain is shown in Figure 9. A second order spatial discretization has been used and the flux discretization has been carried out using Roe-FDS scheme. The computational study has been validated with the experimental data and the results are shown in Figure 9. From Figure 9, it can be seen that the computationally predicted secondary chamber steady state pressures for various primary jet

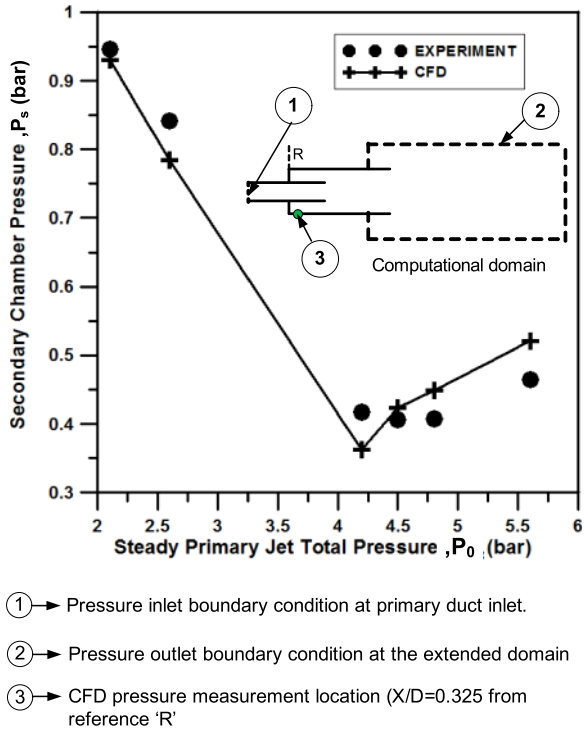


FIG. 9. Comparison of predicted and experimental secondary chamber pressures (L/D = 2.5).

pressure agree reasonably well with the experimentally measured values. The mismatch may be due to the difference between the primary jet total pressure measured in the settling chamber and the pressure, which is actually at the primary jet inlet, and the three dimensional effects.

Figure 10(a) shows the computationally predicted velocity magnitude vectors for case-1 ($P_0$ = 2.1 bars). It clearly exhibits the asymmetric recirculation zones at the top and bottom of the secondary stream, which in turn lead to the asymmetric entrainment of secondary stream. The asymmetric entrainment process eventually leads to a pressure difference across the primary jet boundaries, causing the deflection of primary jet downward or upward as seen in the experiments also. The stream lines for case-1, shown in Figure 10(b), clearly show a bigger recirculation bubble in the diffuser bottom section compared to the diffuser top section and this asymmetry causes the primary jet to deflect.

Pressure data in the upper and lower parts of the secondary chamber (on the same $x$-plane) at un-started condition ($P_0$ = 2.6 bars), shown in Figure 11(a), clearly reveal that the vacuum pressure levels are not at all identical in both the sections. The reason for this can be attributed to the asymmetric entrainment in the un-started mode of ejector operation. Such a situation has a profound influence in the HAT performance, which normally uses the rocket nozzle flow itself as the primary jet, that it would create non uniform vacuum back pressure conditions. This may result in unwanted side loads on the rocket motor due to misaligned thrust vectoring during start-up and produce erroneous test results. Vacuum ejectors used in refrigeration applications mainly operate in the un-started mode and the primary jet deflection can affect the performance of such systems also.

A comparison of the secondary chamber pressure fluctuations (Figure 11(a)) with the corresponding schlieren flow field (Figure 11(b)) shows that the secondary chamber pressure will be higher in the side to which the primary jet deflects. For case-2 ($P_0$ = 2.6 bars), the schlieren picture (Figure 11(b)) shows that the primary jet has been deflected to the diffuser upper wall. A corresponding increase in the vacuum pressure in the secondary chamber upper section compared to the lower section can be observed (Figure 11(a)).

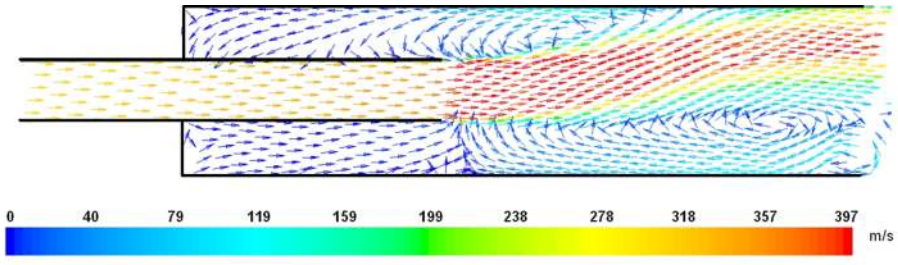


(a) Velocity vector showing the existence of re-circulation bubbles in the diffuser section during un-started mode (case-1).

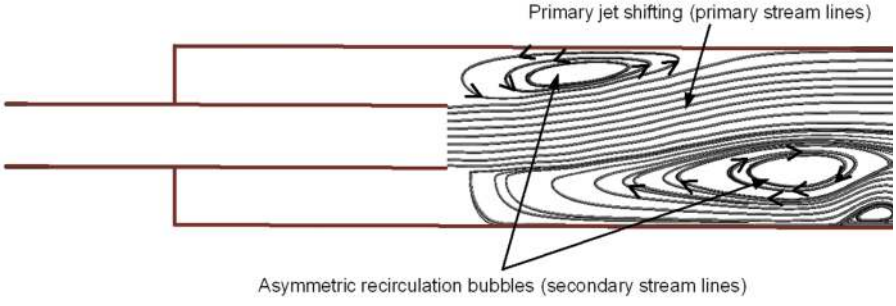


(b) Primary jet stream lines showing the preferential jet attachment to diffuser wall and secondary stream lines showing the asymmetric recirculation bubbles in the diffuser (case-1).

FIG. 10. Computationally predicted flow field for un-started vacuum ejector (case-1).

## B. Phase-2 vacuum ejector operation (L/D = 2.5)

In phase-2, rapid evacuation of the secondary chamber ("B-C" in Figure 5) occurs when the primary jet pressure is ramped above the critical point-2 in Figure 5. Case-4 ($P_0$ = 4.2 bars) represents such a situation. Schlieren picture for case-4 shown in Figure 12(b) illustrates that the primary jet is expanded and reached the diffuser top and bottom walls, indicating started mode operation of the vacuum ejector. Figure 12(a) shows pressure histories in the upper and lower sections of the secondary

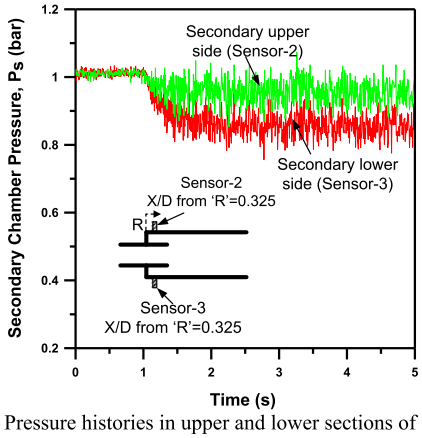


(a) Pressure histories in upper and lower sections of secondary chamber during vacuum ejector start-up (case-2)

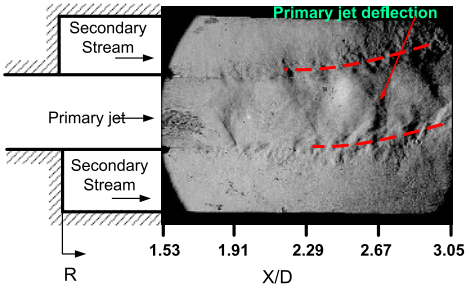


(b) Schlieren image showing the preferential jet attachment of primary jet to the diffuser upper wall (case-2)

FIG. 11. Secondary upper and lower section pressure history and diffuser schlieren flow field (case-2).

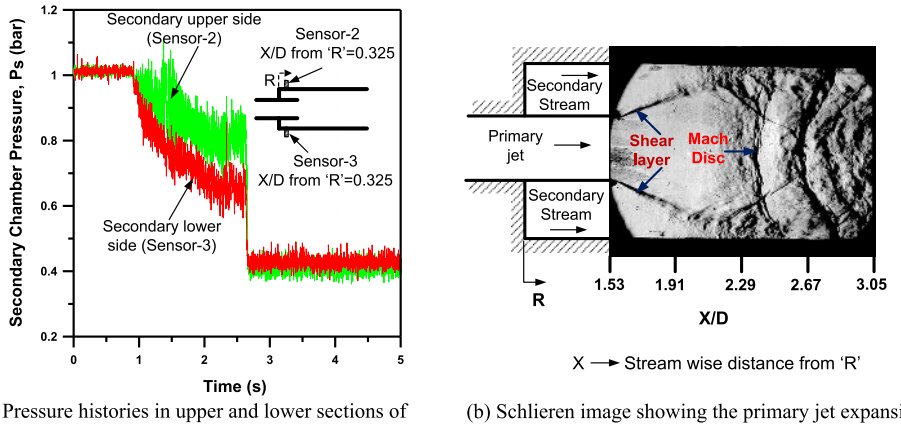


(a) Pressure histories in upper and lower sections of secondary chamber during vacuum ejector start-up (case-4)

(b) Schlieren image showing the primary jet expansion up to the diffuser wall in started mode operation of vacuum ejector (case-4)

FIG. 12. Secondary upper and lower section pressure histories and diffuser schlieren flow field (case-4).

chamber during the primary jet ramping process for case-4. It can be observed that the difference in secondary chamber pressure levels in the upper and lower sections suddenly diminishes with the onset of rapid evacuation stage. Schlieren picture for case-4 (Figure 12(b)) demonstrates that the asymmetric expansion of the primary jet almost vanishes at the vacuum ejector started condition and this is the reason behind the reduction in pressure difference in the secondary chamber.

The computational study carried out for case-4 ($P_0$ = 4.2 bars) also shows results similar to that of the experiment. The stream lines for case-4, shown in Figure 13, reveal that the ejector operates at started condition with primary jet expanding to the diffuser wall. Figure 13 also reveals that the recirculation bubble in the diffuser section, observed early at un-started condition, vanishes with the onset of started mode. The recirculation bubbles can be now seen only in the secondary chamber and are symmetric in nature. The asymmetry in primary jet expansion also vanishes when the ejector is started.

There are other interesting flow features in phase-2, for example, phase-2 can be seen as a "quiet" region compared to phase-1. This transition from a "noisy" phase-1 to a "quiet" phase-2 can be better understood by visualizing the flow characteristics in the diffuser section and comparing it to the secondary chamber pressure history. In this regard, the schlieren images (Figure 14) and the secondary chamber pressure variations (Figure 5) for case-7 ($P_0$ = 6.4 bars) have been compared as explained below.

From the pressure plot (Figure 5), the critical point (point-B) at which the secondary chamber pressure fluctuations diminish is at an elapsed time of 0.408 s from the reference time. The schlieren picture (Figure 14(a)) corresponding to the same time instant reveals that the primary jet has not been fully expanded yet to the diffuser wall. This shows that at point-B, the ejector operates in the un-started mode. Previous studies[22,25] on vacuum ejector report that the pressure fluctuations

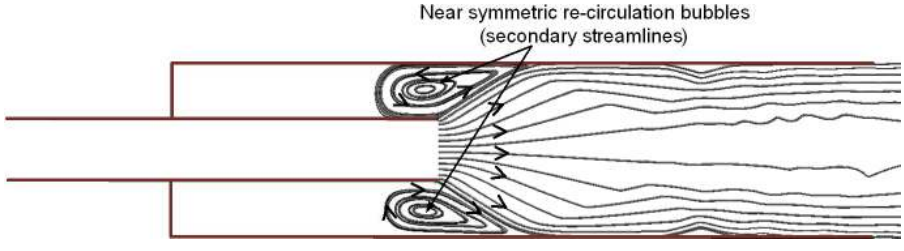


FIG. 13. Primary jet stream lines showing the started mode with no recirculation bubbles in the diffuser and secondary stream lines showing symmetric recirculation bubbles in the secondary chamber (case-4).

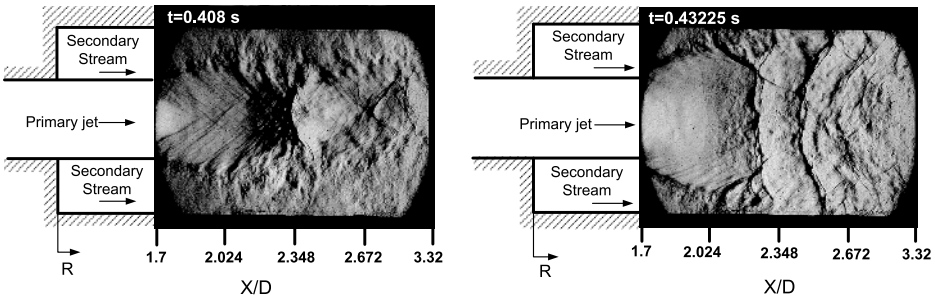


(a) Diffuser schlieren image at the time instant where secondary chamber pressure fluctuations vanish and pressure starts to drop suddenly (point-B in FIG.5)

(b) Diffuser schlieren image at the time instant where secondary sudden evacuation process ends (point-C in FIG.5)

FIG. 14. Diffuser schlieren image at various time instants in phase-2 operation ("B-C" in Fig. 5) for case-7.

in the secondary chamber cease only when the ejector operates in the started mode with oblique shock waves in the diffuser which seal the secondary chamber from the diffuser section. However, the current experiment shows that the secondary chamber pressure fluctuations cease before the onset of started mode vacuum ejector operation. This may be due to the fact that as the primary jet expansion level increases, the area of the secondary flow passage decreases and the secondary jet velocity increases leading to the possibility of secondary flow choking. This prevents the upstream communication of any pressure fluctuations in the downstream diffuser section. Once the upstream communication is blocked, the secondary stream induction will not be affected by the random pressure perturbations in the downstream diffuser section.

From Figure 14(b) which is the schlieren picture corresponding to point-C in Figure 5, it has been observed that the shear layer impinges the diffuser wall and at this instant, the pressure plot shows that the rapid evacuation stage stops. Thus the termination of rapid evacuation stage depicts the onset of started mode operation. The schlieren flow visualization of diffuser section reveals that a Mach reflection (MR) is formed at the location where primary jet expands to the diffuser wall at the onset of started mode operation of the ejector. This is identified as one of the most important characteristic features of any vacuum ejector operating at the onset of started mode.

### C. Phase-3 vacuum ejector operation (L/D = 2.5)

Even though the primary jet total pressure increases from point-3 to point-4 in Figure 5, the vacuum level doesn't seem to be enhanced. The vacuum level remains more or less stable with only a slight reduction. Any further increment in primary pressure from point-4 spoils the already achieved vacuum level. In the started mode, the primary jet just expands to the diffuser wall and a Mach reflection forms due to the deflection of the primary jet. The pressure rise across the Mach stem (normal shock) in the Mach reflection creates an adverse pressure gradient. This will be communicated to the secondary chamber through the subsonic part of the shear layer, leading to a flow reversal into the secondary chamber. However, an increase in primary jet total pressure increases its momentum which in turn enhances the secondary induction. Thus the mass addition into the secondary chamber by the adverse pressure gradient is counteracted by the increased induction rate. This might be the reason for a stable secondary regime between points 3 and 4 of the primary jet pressure window. The "tug of war" between these two processes continues till the primary jet pressure reaches the critical point-4, where a complete isolation of the secondary chamber by the supersonic primary jet occurs.

Figure 15 shows the steady state secondary chamber pressure for various experimental cases. The secondary pressures in Figure 15 have been obtained after achieving various steady state values of primary jet total pressures. It is clearly seen that the secondary chamber pressure initially reduces to a minimum value with increase in primary jet pressure. It then attains a stable regime where only a slight decrease in secondary chamber pressure occurs with the rise in primary jet total pressure.

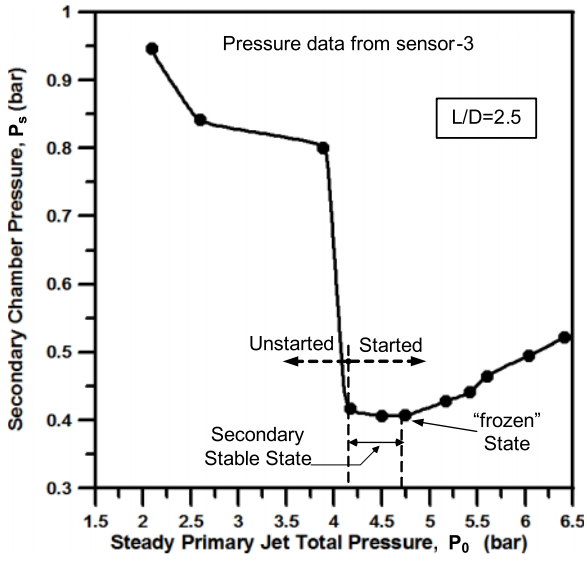


FIG. 15. Steady state secondary chamber pressure corresponding to various primary jet total pressures.

After this stable secondary chamber pressure window, it starts increasing with increasing primary jet pressure. Figure 16 shows the transient secondary pressure-time history for three different primary jet pressure ramping cases. It is seen that for cases with $P_0 = 4.8$ bars and $P_0 = 4.2$ bars, the secondary chamber pressure at steady state remains more or less constant. This confirms the existence of a stable secondary pressure region over a primary jet pressure window after the started mode. Previous studies[22,25] reported that the minimum secondary chamber pressure is attained at the instant when the primary jet attaches to the diffuser wall (started condition) since this creates a blockage to the secondary induction. However, the present study suggests that started condition does not immediately impose a flow blockage to the secondary stream; rather a small induction still happens from the secondary chamber to the diffuser region. Hence it should be noted that there is a

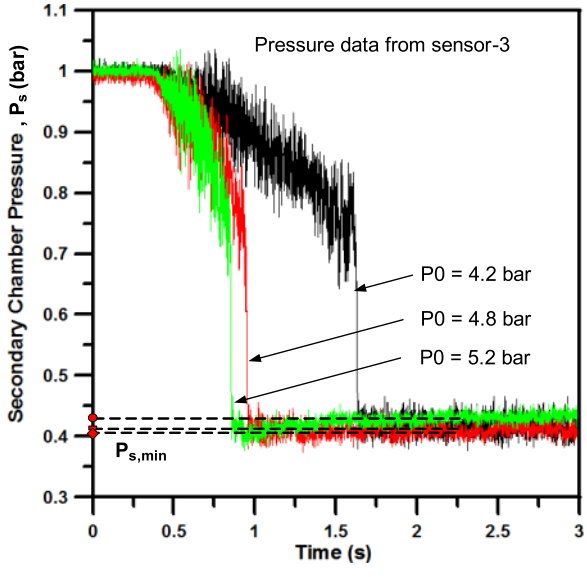


FIG. 16. Secondary pressure-time histories for various primary jet total pressure ramping cases.

clear demarcation between the minimum secondary pressure state and the started mode state, which was previously considered to be the same.[22,25]

### D. Phase-4 vacuum ejector operation (L/D = 2.5)

In phase-4 operation, "D-F" in Figure 5, secondary stream experiences a reverse flow into the secondary chamber which destroys the secondary vacuum level. This can be clearly observed from Figure 15, which shows a rise in secondary pressure after a critical primary jet pressure. This is because, when the primary jet pressure reaches point-4 in Figure 5, the primary jet expansion reaches the maximum possible area ratio (diffuser area ($A_d$)/primary nozzle throat area (A*)) and this completely blocks any secondary induction. As a result of this, the primary jet axial Mach number at the section at which the jet expands to the diffuser wall (diffuser inlet) remains the same even when the primary jet total pressure is raised above point-4, since Mach number depends only on A/A*. This leads to a situation where the incoming primary jet flow becomes "frozen" up to the diffuser inlet. To keep the Mach number (or $P/P_0$) same even when primary jet total pressure is increasing beyond point-4, wall static pressure at the section where primary jet expands to the diffuser wall increases. This causes an adverse pressure gradient for the secondary stream, leading to a flow reversal into the secondary chamber. Since the secondary chamber is now completely closed by the fully expanded primary jet, the latter will not be able to pump out any more secondary fluid. Hence the static pressure in the secondary chamber rises. The flow reversal in phase-3 (C to D in Figure 5) is being compensated by the induction of the secondary stream by the primary jet, whereas the flow reversal in phase-4 (D to F in Figure 5) is not compensated by the induction by the primary jet due to a closed secondary chamber, as shown schematically in Figures 17(a) and 17(b), respectively. The schlieren images corresponding to point-C and point-D in Figure 5 shown in Figures 17(a) and 17(b), respectively, show that the primary jet can undergo further expansion in between the started mode and the frozen state, causing the Mach number to vary.

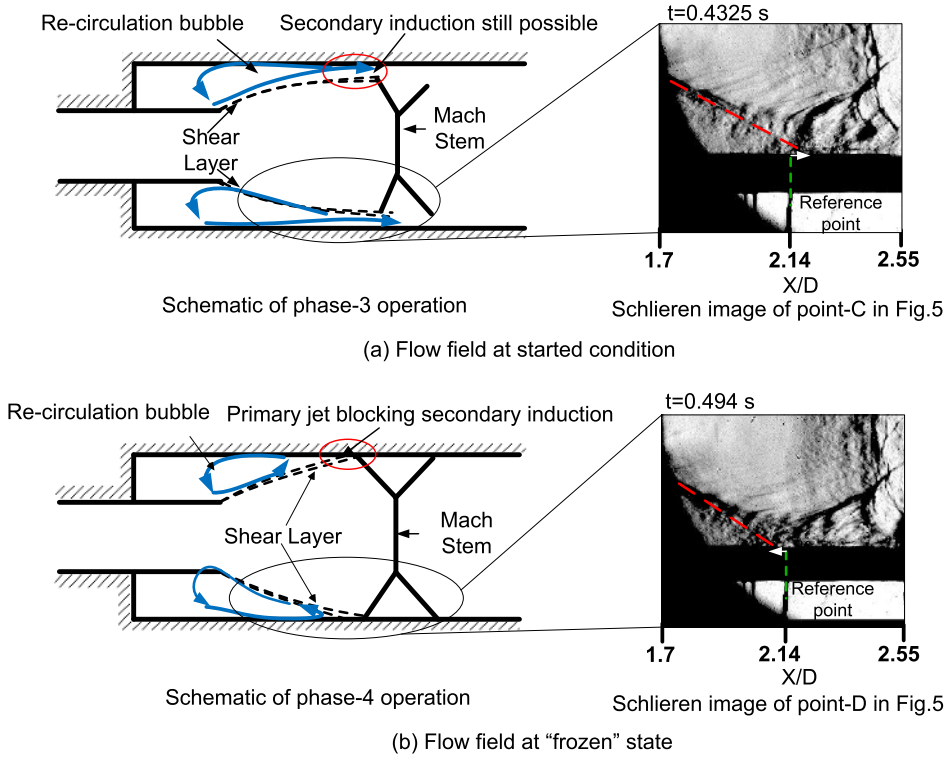


FIG. 17. Flow characteristics at started (point-C) and frozen (point-D) states of vacuum ejector operation.

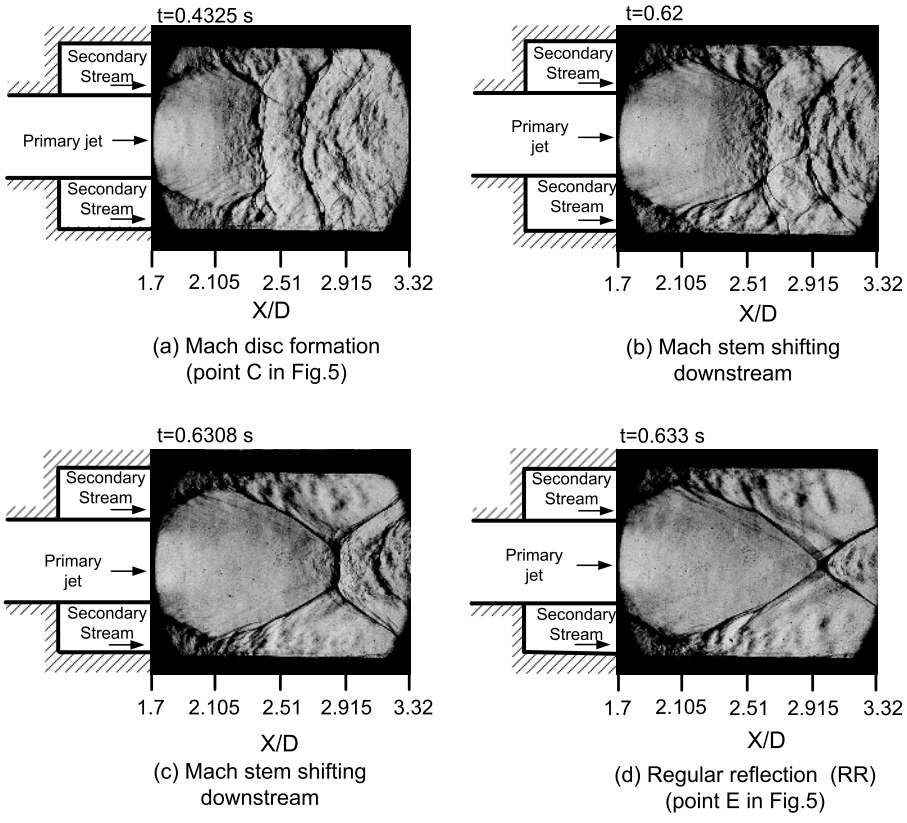


FIG. 18. Diffuser schlieren images at various time instants during phase-4 ("D-F" in Fig. 5) for case-7.

Figure 18 shows the schlieren pictures for case-7 ($P_0$ = 6.4 bars) with primary pressure ramped above the starting mode pressure (point-3 in Figure 5). The pressure data corresponding to each schlieren image can be obtained from Figure 5. An increase in primary jet total pressure above the starting mode critical pressure causes the Mach stem to move downstream with reduction in Mach stem height (Figures 18(a)–18(c)). When the primary jet pressure reaches a critical point, point-5 in Figure 5, the Mach reflection (MR) suddenly transforms to regular reflection (RR), as can be seen from Figure 18(d). It is seen that the secondary chamber pressure varies monotonically from point D to E without reference to any transformation that happens in this flow regime (from Figures 5 and 18). The MR-RR transformation with increase in primary jet pressure may depend on several geometric factors such as diffuser length to its diameter ratio (L/D), diffuser diameter to nozzle exit diameter (D/d), etc. It is also worthwhile to point out here that small amplitude oscillations are also present in the shock structures downstream of the diffuser section. This may also affect the MR-RR transformation. Further investigation is hence needed to understand the mechanism of MR-RR transformation in such ejector flows.

### E. Effects of L/D ratio

It was reported in the previous literatures[21,22,25] that the L/D ratio of the diffuser is one of the major parameters which significantly affects the starting pressure ratios of the vacuum ejectors. It is hence worthwhile to examine the effect of diffuser L/D ratio in the flow structures, especially the shock transformation and the critical pressures. Figure 19 shows the steady state vacuum pressure variations at different primary jet total pressures for vacuum ejectors with various L/D ratios. For varying the L/D, only L is varied while D is kept constant to maintain the same secondary jet thickness. It is observed that when the L/D ratio increases from 2.5 to 5.2, the minimum vacuum pressure in the secondary chamber decreases. This is contradictory to the previous results reported by German

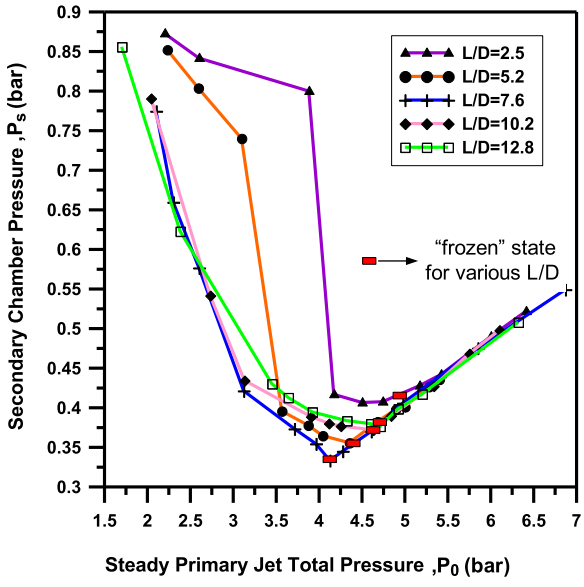


FIG. 19. Secondary pressure for various primary jet total pressures and L/D ratios.

and Bauer[21] in which they observed that the secondary vacuum pressure is not affected by increasing diffuser length. However, Kumaran *et al.*[25] reported slight pressure variations of this kind.

An increase in diffuser length to L/D = 7.6 from L/D = 5.2 further reduces the secondary minimum pressure as well as the primary jet pressure required to achieve the minimum secondary pressure (Figures 19 and 20, respectively). This may be due to the fact that the shock system in the primary jet during the un-started mode gets more length to have multiple shock reflections within the jet. This will enhance the pressure recovery, as shown schematically in Figure 21. An increase in

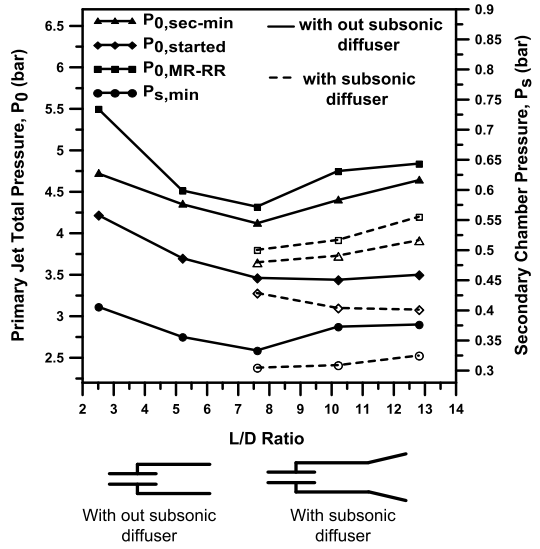


$P_{0,\,sec\text{-}min}$ - Primary total pressure for achieving minimum secondary pressure

$P_{0,started}$ - Primary total pressure for attaining started mode

$P_{0,MR\text{-}RR}$ - Primary total pressure for MR-RR transformation

$P_{s,min}$ - Minimum secondary chamber pressure

FIG. 20. Variations in different critical pressures with respect to diffuser length.

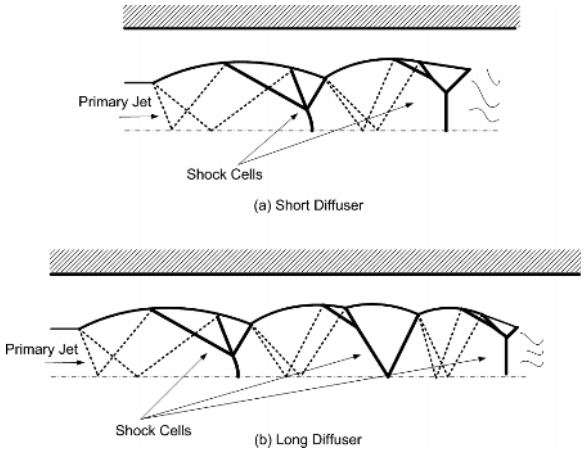


FIG. 21. Schematic of shock cell characteristics with increases in diffuser length.

pressure recovery reduces the primary jet total pressure required to achieve the diffuser inlet Mach number at started condition[21,22,25] (as in the case of supersonic wind tunnels with diffusers) and this in turn reduces the static pressure at diffuser inlet. The reduction in primary jet static pressure at the section where primary jet expands to the diffuser wall (diffuser inlet) will reduce secondary chamber pressure also, consequently, leading to a higher vacuum level. This shock assisted pressure recovery reaches a limit when the diffuser length reaches a critical value, since with sufficient diffuser length, the shock trains will yield a subsonic flow. As a result of this, any increase in diffuser length from this stage will not make any appreciable change in the primary jet total pressure required for started condition as observed in Figure 20.

When L/D is increased from 7.6 to 10.2 and then to 12.8, the minimum pressure attained in the secondary chamber is seen to be increasing as shown in Figures 19 and 20. This suggests that the minimum vacuum condition initially decreases with increase in diffuser length, reaches a minimum value, and there after increases with increase in diffuser length. Since the pressure variations with L/D increase are seemingly small, the error bands for different cases have been calculated to estimate the measurement uncertainties in the reported secondary chamber pressure variations

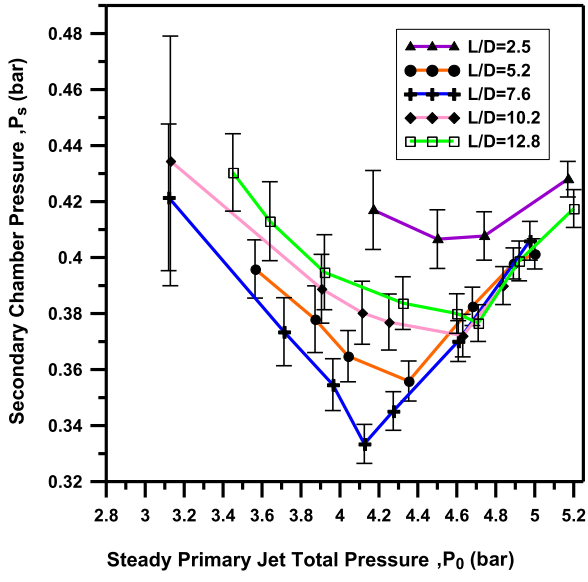


FIG. 22. Standard deviations (error bands) of the secondary chamber pressure data in Fig. 19.

and are shown in Figure 22. It can be seen from the error bands of L/D = 10.2 and L/D = 7.6 that the increase in minimum secondary pressure above a critical limit is not due to measurement uncertainties but due to the flow characteristics associated with the L/D increase.

What follows is an explanation of the phenomenon discussed above. For L/D = 7.6, a primary jet total pressure of 4.12 bars creates the maximum possible expansion level for the primary jet ("frozen" state) and this creates the minimum secondary chamber pressure. Now if the diffuser length is increased further to L/D = 10.2 with the primary jet total pressure unchanged, the flow has to overcome the additional friction caused by the increase in diffuser length. In sufficiently long diffusers (for example, L/D = 10.2), the shock train terminates somewhere downstream of the diffuser, producing a subsonic flow. The subsonic flow in the remaining straight diffuser portion will be identical to that of subsonic Fanno flow. As per Fanno theory,[33] addition of diffuser length in subsonic flow necessitates the flow to move to a new Fanno line with a reduced mass flux, if the pressure ratio is kept the same. The pressure ratio[33] is defined as the ratio of exit ambient pressure (which remains same for both L/D = 10.2 and L/D = 7.6) to the total pressure in the diffuser section where subsonic flow first occurs. The diffuser section where the subsonic flow first occurs is termed as the Fanno duct entrance. This is schematically shown in Figure 23. For the case with L/D = 10.2, shifting to a new Fanno line with a reduced mass flux is not possible. This is due to the fact that the mass flow rate through the diffuser will be same as the primary nozzle mass flow rate. For both L/D cases (7.6 and 10.2), the nozzle throat area and the primary jet total pressure remain the same with primary nozzle operating at choked condition. Hence the diffuser mass flow rate for L/D = 10.2 will be same as that of L/D = 7.6. The only option left out to push the same mass flow with added diffuser length (L/D = 10.2) is to increase the pressure ratio by increasing the total pressure at the Fanno duct entrance. A higher total pressure at Fanno duct entrance region is generated by adjusting the properties across the Mach stem which is nearly a normal shock located at the diffuser inlet section (shown schematically in Figure 23). This is achieved by reducing the total pressure loss across the Mach stem by reducing the shock upstream Mach number ($M_x$). For a constant primary jet total pressure ($P_0$), the static pressure upstream of the Mach stem ($p_x$) increases with reduction in upstream shock Mach number (from the isentropic relation, $P_0/P_x = f(M_x)$). The flow is capable of doing these adjustments because the ejector operation is still in between points C and D (phase-3) in Figure 5, where the diffuser inlet Mach number can change. The increase in primary jet static pressure upstream of the shock wave eventually increases the secondary chamber pressure for L/D = 10.2. Hence in between the started mode and the frozen state, the secondary chamber pressure for L/D = 10.6 will be higher compared to L/D = 7.6 even if both cases are operated at same primary jet total pressures. At L/D = 7.6, the shock assisted pressure recovery dominates the subsonic Fanno effect since the subsonic duct length is small. However, for L/D = 10.2, the shock assisted pressure recovery is significantly counter-acted by the Fanno effect, which increases the total pressure required for achieving the minimum secondary chamber pressure ("frozen" state). This in turn increases the secondary chamber pressure and thereby spoiling the vacuum level.

To justify the above arguments, a qualitative picture of the jet expansion is shown in Figure 24. The shock upstream Mach number reduction and the static pressure ($p_x$) increase can be observed

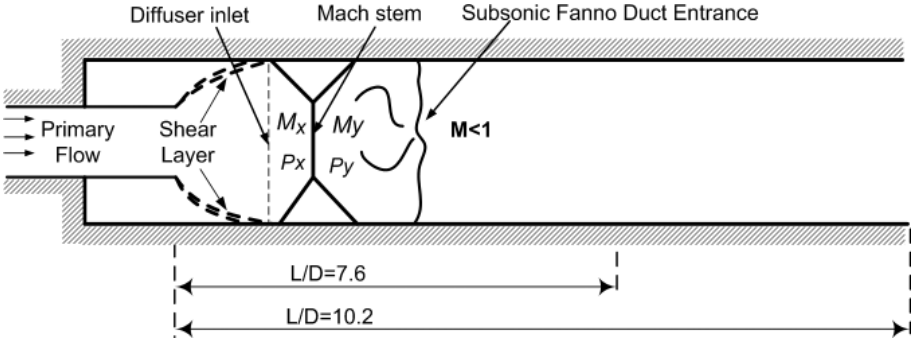


FIG. 23. Schematic showing subsonic Fanno duct in diffuser.

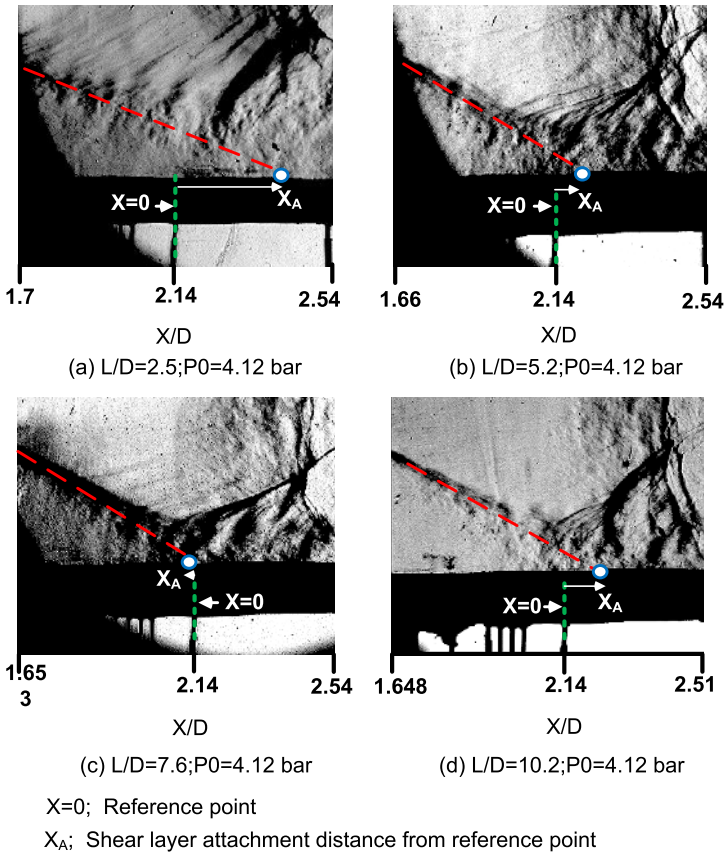


FIG. 24. Schlieren images showing the primary jet expansion levels for various L/D ratios.

from the amount of primary jet expansion from Figure 24. A higher static pressure at the diffuser inlet results in less expansion of primary jet at diffuser inlet. Figure 24 shows the comparison of primary jet expansion level for cases with various L/D ratios with the same primary jet total pressure. The jet expansion is visualized by defining a length "$X_A$" between a reference point 'X' and the diffuser inlet. It can be observed that when diffuser length increases from L/D = 2.5 to L/D = 7.6 (Figures 24(a)–24(c)), the primary jet expansion level increases ($X_A$ decreases). This indicates that in this range of diffuser lengths, the static pressure at the diffuser inlet reduces with increase in diffuser length. This in turn reduces the secondary chamber pressure. However, when diffuser length is increased in the range of L/D = 7.6 to 10.2 (Figure 24(d)), the primary jet expansion level reduces ("$X_A$" increases). This can be noted as a static pressure rise at the diffuser inlet and in the secondary chamber. Thus it is obvious from the schlieren pictures that as the diffuser length increases up to a certain critical level, the minimum achievable secondary pressure decreases (vacuum increases) due to the shock assisted pressure recovery. When diffuser length increases above this limit, Fanno effects become dominant which in turn increases the minimum achievable secondary chamber pressure (vacuum decreases).

Another interesting phenomenon which can be seen from Figure 19 is that the secondary pressure variation becomes independent of diffuser length once the diffuser inlet attains the frozen state (minimum secondary chamber pressure). For various L/D ratios, the frozen state is attained at different primary jet total pressures due to pressure recovery and Fanno effects. Once the frozen state is attained, the static pressure at the diffuser inlet is then decided solely by the primary jet total pressure. From the isentropic relation $P/P_0 = f(M = \text{constant})$, it can be noted that after the frozen state, the static pressure increases linearly with respect to $P_0$, so is the pressure variation in the secondary chamber. Hence all the plots in Figure 19 eventually collapse to a single straight line.

The attainment of constant Mach number (frozen state) for various L/D ratios also implies that from this point onwards, the frictional effects due to length addition cannot influence the flow upstream of the diffuser inlet. Now the enhancement of total pressure at the subsonic Fanno duct entrance for the increased L/D ratios may be achieved by adjusting the shock characteristics downstream of diffuser inlet since the upstream flow reaches a frozen state.

All the critical pressures for various L/D ratios are plotted in Figure 20. It can be observed from Figure 20 that the critical primary jet total pressures required for shock transformation also show a similar "initial decrease then increase" trend with increase in diffuser length. It was observed that the minimum secondary chamber pressure, started mode critical pressure, and the critical pressure for MR-RR transformation can be further reduced by adding a subsonic diffuser as shown in Figure 20. The subsonic flow produced by the shock trains in the straight diffuser can be further decelerated through the diffusion action in the subsonic diffuser. This will enhance the pressure recovery and hence reduces the various critical pressures.

The details of various vacuum generation stages reported in the current work will be useful in identifying the primary jet operating pressures for having better performance of vacuum ejector at both started and un-started modes. At un-started mode, a better performance can be obtained if majority of vacuum generation process is progressed through the "quiet second stage". This can be achieved by a rapid primary jet pressure ramping up to the secondary choked state so that the secondary fluctuations can be avoided quickly. It is also understood from the present study that there exists a particular primary jet pressure window for a specific vacuum ejector geometry over which a minimum secondary vacuum state can be achieved. A prior determination of this pressure window helps in reducing the operational cost of vacuum ejectors. The present study also suggests that the diffuser length should be carefully chosen in such a way that the pressure recovery and Fanno effects are maximized and minimized, respectively, so that maximum vacuum level can be attained with a minimum primary jet pressure.

In order to have a more detailed understanding of the pressure recovery effects through shock system and the Fanno effect for various L/D ratios, a more comprehensive study involving pressure measurements across the shock systems and schlieren flow visualization further downstream of the diffuser section is required, which is planned as a future study. Moreover, in the present work, a simple 2-D straight duct nozzle is used to generate the primary jet while the actual geometry of the ejector systems being used in HAT facility is 3-D with a C-D nozzle for generating the primary jet. Considering the above two aspects, the present work is hence planned to be extended to derive empirical relations that are useful for the actual systems.

## IV. CONCLUSIONS

Experimental study on a vacuum ejector reveals that the secondary chamber vacuum generation process exhibits different stages of evacuation with nonuniform rates. Initial starting process was subjected to large scale flow oscillations in the secondary chamber which was then followed by a "quiet" rapid evacuation state with no notable fluctuations. Schlieren images corresponding to the onset of the rapid evacuation stage reveal that the "quiet" evacuation state is not an indication of the started mode operation (primary jet expansion up to the diffuser wall) of the ejector as reported previously but is due to the secondary flow choking just before the started mode operation. It is also found that a stable vacuum level exists in the secondary chamber for a range of primary jet operating pressures. This suggests that the started mode operation does not create a sudden flow blockage to secondary entrainment as reported previously. At the onset of started mode operation, the diffuser section exhibits a Mach reflection (MR). With further increase in primary jet total pressure, the MR stretches and eventually transforms into a Regular Reflection (RR). It is observed that the vacuum generation in the secondary chamber in the un-started mode is mostly asymmetric owing to the primary jet deflection to any one of the diffuser walls due to the asymmetric development of the re-circulation bubbles. This asymmetric vacuum pressure condition diminishes with the onset of started mode operation. The current study also reveals that with increase in diffuser length, the minimum possible secondary vacuum, primary jet pressure for attaining the minimum

vacuum, and the primary jet pressure for MR-RR transition decrease initially and then increase. The decrease and increase in the critical pressure are attributed to shock assisted pressure recovery and the Fanno flow effects, respectively. These critical primary pressures as well as the secondary vacuum level are found to be further reduced by adding a subsonic diffuser, since it enhances the pressure recovery.


[1] J. H. Keenan and E. P. Neumann, "A simple air ejector," Trans. ASME: J. Appl. Mech. **64**, 75–81 (1942).
[2] D. E. Paxson and K. T. Dougherty, "Ejector enhanced pulsejet based pressure gain combustors: An old idea with a new twist," 41st Joint Propulsion Conference and Exhibit, Arizona, USA, 10–13 July 2005.
[3] J. M. Abdulateef, K. Sopian, M. A. Alghoul, and M. Y. Sulaiman, "Review on solar-driven ejector refrigeration technologies," Renewable Sustainable Energy Rev. **13**, 1338–1349 (2009).
[4] B. J. Huang, C. B. Jiang, and F. L. Hu, "Ejector performance characteristics and design analysis of jet refrigeration system," Trans. ASME: J. Fluids Eng. **107**, 792–802 (1985).
[5] K. Chunnanond and S. Aphornratana, "Ejectors: Applications in refrigeration technology," Renewable Sustainable Energy Rev. **8**, 129–155 (2004).
[6] M. Alperin and J.-J. Wu, "Thrust augmenting ejectors. Part I," AIAA J. **21**(10), 1428–1436 (1983).
[7] M. Alperin and J.-J. Wu, "Thrust augmenting ejectors. Part II," AIAA J. **21**(12), 1698–1706 (1983).
[8] K. K. Ahuja, "Mixing enhancement and jet noise reduction through tabs plus ejectors," AIAA Paper No. 93-4347, 1993.
[9] J. H. Keenan, E. P. Neumann, and F. Lustwerk, "An investigation of ejector design by analysis and experiment," Trans. ASME: J. Appl. Mech. **72**, 299–309 (1950).
[10] J. Fabri and J. Paulon, "Theory and experiment on supersonic air-to-air ejectors," NACA Technical Memorandum 1410, 1958.
[11] A. L. Addy, J. C. Dutton, and C. D. Mikkelensen, "Supersonic Ejector-Diffuser Theory and Experimen," Report No. ADP000536, University of Illinois, Urbana, 1981.
[12] J. C. Dutton, C. D. Mikkelsen, and A. L. Addy, "A theoretical and experimental investigation of the constant area supersonic-supersonic ejector," AIAA J. **20**(10), 1392–1400 (1982).
[13] B. J. Huang, J. M. Chang, C. P. Wang, and V. A. Petrenko, "A 1-D analysis of ejector performance," Int. J. Refrig. **22**, 354–364 (1999).
[14] B. Mandell, B. L. Mc Farland, R. E. Nelson, and G. O. Patmor, "Scale model testing of 90 deg Supersonic turn ejector systems for altitude simulation," J. Spacecr. Rockets **1**(1), 108–111 (1964).
[15] T. D. Derick, "A general simulation of an air ejector diffuser system," M.S. thesis, University of Tennessee, Knoxville, 2010.
[16] A. Mittal, G. Rajesh, V. Lijo, and H. D. Kim, "Starting transients in vacuum ejector-diffuser system," J. Propul. Power **30**(5), 1213–1223 (2014).
[17] W. L. Jones, H. G. Price, Jr., and C. F. Lorenzo, "Experimental study of zero-flow ejectors using gaseous nitrogen," NASA Technical Note D-230, 1960.
[18] R. C. Bauer and R. C. German, "Some Reynolds number effects on the performance of ejectors without induced flow," Technical Report AEDC-AEDC-TN-61–87, 1961.
[19] R. C. Bauer and R. C. German, "The effect of second throat geometry on the performance of ejectors without induced flow," Technical Report AEDC-AEDC-TN-61–133, 1961.
[20] C. J. Wojciechowski and P. G. Anderson, "Parametric analysis of diffuser requirements for high expansion ratio space engine," NASA Technical Note LMSC-11REC TR D784489, 1981.
[21] R. C. German and R. C. Bauer, "Effects of diffuser length on the performance of ejectors without induced flow," Technical Report AEDC-AEDC-TN-61–89, 1961.
[22] K. Annamalai, K. Visvanathan, V. Sriramulu, and K. A. Bhaskaran, "Evaluation of the performance of supersonic exhaust diffuser using scaled down models," Exp. Therm. Fluid Sci. **17**, 217–229 (1998).
[23] A. H. Shapiro, *The Dynamics and Thermodynamics of Compressible Fluid Flow* (The Ronald Press Company, New York, 1953).
[24] R. K. Ashok, S. Sankaran, K. Srinivasan, and T. Sundararajan, "Effects of vacuum chamber and reverse flow on supersonic exhaust diffuser starting," J. Propul. Power **31**(2), 750–754 (2015).
[25] R. M. Kumaran, P. K. Vivekanand, T. Sundararajan, K. Kumaresan, and D. R. Manohar, "Optimization of second throat ejectors for high-altitude test facility," J. Propul. Power **25**(3), 697–706 (2009).
[26] V. Lijo, H. D. Kim, G. Rajesh, and T. Setoguchi, "Numerical simulation of transient flows in a vacuum ejector-diffuser system," Proc. Inst. Mech. Eng., Part G **224**(7), 777–786 (2010).
[27] B. H. Park, J. H. Lee, and W. Yoon, "Studies on the starting transient of a straight cylindrical supersonic exhaust diffuser: Effects of diffuser length and pre-evacuation state," Int. J. Heat Fluid Flow **29**(5), 1369–1379 (2008).
[28] H. D. Kim and J. S. Lee, "An experimental study of supersonic ejector for a vacuum pump," in *Proceedings of The Korean Society of Mechanical Engineers, Annual Fall Meeting* (Korean Society of Mechanical Engineering, Seoul, Republic of Korea, 1994), Vol. B, pp. 520–525.
[29] B. H. Park, J. H. Lim, and W. Yoon, "Fluid dynamics in starting and terminating transients of zero-secondary flow ejector," Int. J. Heat Fluid Flow **29**(1), 327–339 (2008).
[30] D. Drikakis, "Bifurcation phenomena in incompressible sudden expansion flows," Phys. Fluids **9**(1), 76–87 (1997).
[31] W. Cherdron, F. Durstand, and J. H. Whitelaw, "Asymmetric flows and instabilities in symmetric ducts with sudden expansions," J. Fluid Mech. **84**(1), 13–31 (1978).
[32] F. Durst, J. C. F. Pereirat, and C. Tropea, "The plane symmetric sudden-expansion flow at low Reynolds numbers," J. Fluid Mech. **248**, 567–581 (1993).
[33] R. D. Zucker and O. Biblarz, *Fundamentals of Gas Dynamics* (John Wiley & Sons, New Jersey, 2002).